07

Spontaneous four-photon mixing in ghost imaging

© A.V. Belinsky, V.V. Vasilkov

Moscow State Universit,
119991 Moscow, Russia

e-mail: belinsky@inbox.ru, soc.ggt@gmail.com

Received August 27, 2022
Revised October 18, 2022
Accepted December 10, 2022

A generalization of the calculation of the formation of ghost images in the course of backward four-photon mixing to the real situation of non-planar spatially limited pumping, which has a Gaussian profile of the fundamental laser mode, is developed, taking into account the specifics of the formation of phantom images. Computer images have been obtained that make it possible to estimate the spatial resolution of the systems. A relatively simple equivalent scheme for describing the process is proposed, which shows that the effect of diffraction in nonlinear systems is similar to its role in ordinary linear optics with a limited aperture. A fiber-optic version of the formation of ghost images is proposed, suitable for the study of hard-to-reach cavities and organs of the human body, which allow the introduction of a thin fiber bundle there.

Keywords: quantum entangled states, quantum images, optical systems, ghost images, quantum measurements.

DOI: 10.21883/EOS.2023.01.55517.4060-22

Introduction

Recently, there has been a significant increase in interest in systems for obtaining and forming phantom images [1–36]. This is due to a number of their advantages over conventional images, especially when working with biological objects, when a gentle mode of irradiation of the studied living beings is important. There are also interesting options for exploring hard-to-reach areas, for example, closed cavities, using fiber optics, if it is possible to launch a fiber bundle there [11–30].

In the recent paper [10] it is shown that when forming quantum phantom images, the use of counter four-photon mixing can give significant advantages compared to the traditionally used three-photon process [1]. This is due to the fact that due to the possible isotropy of the nonlinear medium, diffraction restrictions are removed due to the condition of phase synchronism and the corresponding limit of the angular aperture of light beams. A small aperture destructively affects the quality of images due to their diffraction blurring.

In the mentioned paper [10], the constancy of the gain increment for a wide angular spectrum of light beams involved in the formation of phantom images during a counter four-photon process is demonstrated, but only in the approximation of plane pumping. At the same time, a logical question arises: what will happen in the real case of Gaussian laser pumping? Therefore, we tried to solve this problem. The results are described below.

1. Setup scheme

In Fig. 1, a nonlinear medium with cubic nonlinearity from above and below is irradiated by oncoming laser pumping beams p and q. The signal and idle beams generated in this case s and i also have strictly opposite directions and illuminate the object O and the CCD photodetector matrix. Working in parallel beams of rays avoids a number of aberrations due to the symmetry of the optical system at a single, or rather minus a single, magnification of [8]. But at the same time it is necessary to install two identical lenses L, focusing the generated radiation. In Fig. 1, they are symbolically shown as convex spherical lateral surfaces of a nonlinear medium.

The signal beam illuminates the CCD, and the idle — integrating single-pixel BD detector, which captures all photons penetrating the object, regardless of their localization, of course, taking into account its quantum efficiency and the transparency of the object O. The coincidence scheme C highlights only simultaneous detection in the photon counting mode. These signals, taking into account the spatial position of the triggered detector of the CCD matrix, are sent to the computer forming the image of the object, and thus the standard algorithm for constructing phantom images [31] is implemented.

2. General relations

To obtain quantum equations describing a counter four-photon process, we use the field momentum operator by analogy with how it is done in [37] for three-photon parametric interaction. In our case it is equal to

$$\hat{G} = \int \Bigg(-i\hbar\chi^{(3)} A_p(\mathbf{r}) A_q(\mathbf{r}) \hat{A}_s^{\dagger}(\mathbf{r}) \hat{A}_i^{\dagger}(\mathbf{r}) + H.c. + \frac{\hbar}{2k} \sum_{j=i,s} \frac{\partial \hat{A}_j^{\dagger}(\mathbf{r})}{\partial \mathbf{r}_{\perp}} \frac{\partial \hat{A}_j(\mathbf{r})}{\partial \mathbf{r}_{\perp}} \Bigg) d\mathbf{r}_{\perp},$$

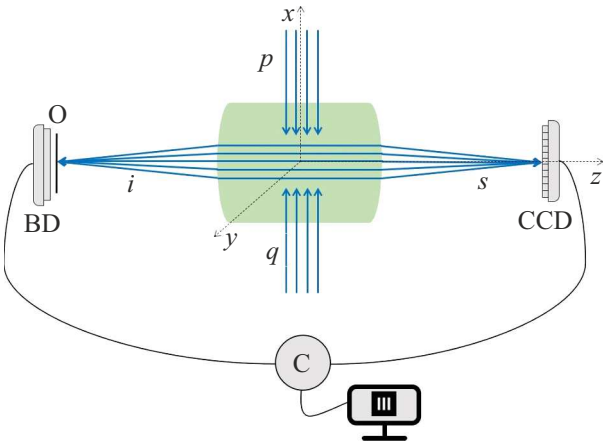

Figure 1. Phantom image formation scheme: p and q — counter laser pumping beams in a nonlinear medium with cubic nonlinearity (in center), s and i — signal and idle beams, O — partially transparent investigated object, BD — integrating detector that does not have spatial resolution, CCD — photodetector matrix operating in photon counting mode, like BD, C — a coincidence circuit connected to a computer that reproduces the image of the object O.

where $H.c. = i\hbar\chi^{(3)}A_p^*(\mathbf{r})A_q^*(\mathbf{r})\hat{A}_i(\mathbf{r})\hat{A}_s(\mathbf{r})$ — Hermitian conjugation. Field operators

$$\hat{A}_j(\mathbf{r}_\perp, z) = \int_{-\infty}^{\infty} \hat{a}_j(\mathbf{k}_j, z)\exp[i\mathbf{r}\mathbf{k}_\perp]d^2\mathbf{k}_\perp,$$

$$\hat{A}_j^\dagger(\mathbf{r}_\perp, z) = \int_{-\infty}^{\infty} \hat{a}_j^\dagger(\mathbf{k}_\perp, z)\exp[-i\mathbf{r}\mathbf{k}_\perp]d^2\mathbf{k}_\perp,$$

where $\hat{a}_j$ and $\hat{a}_j^\dagger$ — respectively, the photon destruction and generation operators in the Heisenberg representation, integration is carried out in the transverse plane $\mathbf{r}_\perp = \{x, y\}$, z — longitudinal coordinate, k_j — wave number, we consider the degenerate case $k_s = k_i = k$, $\chi^{(3)}$ — coefficient proportional to cubic nonlinearity. The last term of the momentum operator describes diffraction. An approximation of a given classical pump is used — its counter beams are marked with indices p, q, and $A_p(\mathbf{r})$, $A_q(\mathbf{r})$ — classical complex amplitudes. The indices s, i correspond to the signal and idle wave, $\mathbf{k}_\perp = (k_x, k_y)$ — the transverse component of the wave vector.

Let us write the derivatives in the direction $\mathbf{r}_\perp = \mathbf{r}(x, y)$ using the definition

$$\frac{\partial\hat{A}_j(\mathbf{r}_\perp)}{\partial\mathbf{r}_\perp} = (\nabla_\perp\hat{A}_j\mathbf{e}_{\mathbf{r}_\perp}), \quad \frac{\partial\hat{A}_j^\dagger(\mathbf{r}_\perp)}{\partial\mathbf{r}_\perp} = (\nabla_\perp\hat{A}_j^\dagger\mathbf{e}_{\mathbf{r}_\perp}).$$

Then

$$\hat{G} = \int\Bigg(-i\hbar\chi^{(3)}A_p(\mathbf{r})A_q(\mathbf{r})\hat{A}_s^\dagger(\mathbf{r})\hat{A}_i^\dagger(\mathbf{r}) + H.c. + \frac{\hbar}{2k}\sum_{j=i,s}(\nabla_\perp\hat{A}_j^\dagger\mathbf{e}_{\mathbf{r}_\perp})(\nabla_\perp\hat{A}_j\mathbf{e}_{\mathbf{r}_\perp})\Bigg)dxdy.$$

Taking into account the evolution equation:

$$i\hbar\frac{\partial\hat{A}_{s,i}(\mathbf{r})}{\partial z} = [\hat{G}, \hat{A}_{s,i}(\mathbf{r})]$$

and the switching relations:

$$[\hat{A}_j^\dagger(\mathbf{r}), \hat{A}_l(\mathbf{r}')] = -\delta_{jl}\delta(\mathbf{r}-\mathbf{r}'), \quad [\hat{A}_j(\mathbf{r}), \hat{A}_l(\mathbf{r}')] = 0$$

we obtain

$$\begin{cases}\frac{\partial\hat{A}_s(\mathbf{r})}{\partial z} + \frac{i}{2k}\Delta_\perp\hat{A}_s = \chi^{(3)}A_p(\mathbf{r})\hat{A}_q(r)\hat{A}_i^\dagger(\mathbf{r}),\\ \frac{\partial\hat{A}_i^\dagger(\mathbf{r})}{\partial z} - \frac{i}{2k}\Delta_\perp\hat{A}_i = -\chi^{(3)}A_p(\mathbf{r})\hat{A}_q(r)\hat{A}_s(\mathbf{r}).\end{cases} \quad (1)$$

Intermediate transformations are used here:

$$i\hbar\frac{\partial\hat{A}_s}{\partial z} = \int\Bigg(-i\hbar\chi^{(3)}[A_pA_q\hat{A}_s^\dagger\hat{A}_i^\dagger, \hat{A}_s] + [H.c., \hat{A}_s] + \frac{\hbar}{2k}\sum_{j=i,s}[(\nabla_\perp\hat{A}_s^\dagger\mathbf{e}_{\mathbf{r}'_\perp})(\nabla_\perp\hat{A}_s\mathbf{e}_{\mathbf{r}'_\perp}), \hat{A}_s]\Bigg)d\mathbf{r}'_\perp$$

$$= i\hbar\chi^{(3)}A_pA_q\hat{A}_i^\dagger + \frac{\hbar}{2k}\Delta_\perp\hat{A}_i.$$

System of equations (1) was also used in the paper [10], but was given there without a conclusion by analogy with the system of classical equations for complex amplitudes [38].

Given the small thickness of the nonlinear medium compared to the optical path of the signal and idle beams, the diffraction term $\frac{i}{2k}\Delta_\perp canbeneglected\hat{A}_i$, i.e.

$$\begin{cases}\frac{\partial\hat{A}_s}{\partial z} = \chi^{(3)}A_pA_q\hat{A}_i^\dagger,\\ \frac{\partial\hat{A}_i}{\partial z} = \chi^{(3)}A_pA_q\hat{A}_s^\dagger.\end{cases} \quad (2)$$

Pumping usually has a Gaussian profile. Again, due to the small size of the nonlinear medium, it can be considered cylindrical:

$$A_{p,q}(\mathbf{r}) = A_{p,q}(x, y, z) = A\exp\left[-\left(\frac{y^2}{2\sigma_y^2} + \frac{z^2}{2\sigma_z^2}\right)\right],$$

where σ — defines the beam width.

2.1. Matrices of operators $\hat{A}^\dagger$ and $\hat{A}$

Let us define the vacuum state as a set of all possible plane modes: $|0\rangle = \prod_{\mathbf{k}_\perp}|0\rangle_{\mathbf{k}_\perp}$. Then for field operators

$$\hat{A}^\dagger(\mathbf{r}_\perp, z)|0\rangle = \int_{-\infty}^{\infty}\hat{a}^\dagger(\mathbf{k}_\perp, z) \times\exp[-i\mathbf{r}_\perp\mathbf{k}_\perp]d^2\mathbf{k}_\perp\prod_{\mathbf{k}_\perp}|0\rangle_{\mathbf{k}_\perp} = |1\rangle,$$

where is the tensor product of $\mathbf{k}_\perp$, and by $|1\rangle$ we mean the entire last integral. One can also complete a definition:

$$\hat{A}^\dagger(\mathbf{r}_\perp, z)|0\rangle = \sqrt{1}|1\rangle, \quad \hat{A}(\mathbf{r}_\perp, z)|1\rangle = \sqrt{1}|0\rangle,$$

so, by analogy with [39], construct matrices of operators $\hat{A}^\dagger$, $\hat{A}$ and state vectors $|0\rangle$, $|1\rangle$:

$$\hat{A} = \begin{pmatrix} 0 & \sqrt{1} \\ 0 & 0 \end{pmatrix}, \ \hat{A}^\dagger \begin{pmatrix} 0 & 0 \\ \sqrt{1} & 0 \end{pmatrix}, \ |0\rangle = \begin{pmatrix} 1 \\ 0 \end{pmatrix}, \ |1\rangle = \begin{pmatrix} 0 \\ 1 \end{pmatrix}.$$

Or for matrix elements:

$$(\hat{A})^{jk} = \begin{cases} \sqrt{1}, & k - j = 1 \\ 0, & k - j \neq 1 \end{cases},$$

$$(\hat{A}^\dagger)^{jk} = \begin{cases} \sqrt{1}, & j - k = 1 \\ 0, & j - k \neq 1 \end{cases}, \ j, k = \overline{1, 2},$$

$$|n\rangle^j = \begin{cases} 1, & j = n + 1 \\ 0, & j \neq 0 + 1 \end{cases}, \ j = \overline{1, 2}.$$

2.2. General Hilbert space

The state vectors of the bundles s and i are denoted by $|n\rangle_s$, $|m\rangle_i$. The total Hilbert space H is defined by the tensor product $H = H_s \otimes H_i$.

Let us consider $|nm\rangle = |n\rangle_s \otimes |m\rangle_i$ and write down the lower states:

$$|00\rangle = \begin{pmatrix} 1 \\ 0 \\ 0 \\ 0 \end{pmatrix}, \ |01\rangle = \begin{pmatrix} 0 \\ 1 \\ 0 \\ 0 \end{pmatrix}, \ |10\rangle = \begin{pmatrix} 0 \\ 0 \\ 1 \\ 0 \end{pmatrix}, |11\rangle = \begin{pmatrix} 0 \\ 0 \\ 0 \\ 1 \end{pmatrix}, \tag{3}$$

for matrix elements

$$|nm\rangle^j = \begin{cases} 1, & j = 2n + m + 1 \\ 0, & j \neq 2n + m + 1 \end{cases}, \ j = \overline{1, 4}.$$

In general Hilbert space:

$$\hat{A}_s = (\hat{A}_s \otimes \hat{I}_i) = \begin{pmatrix} 0 & 0 & \sqrt{1} & 0 \\ 0 & 0 & 0 & \sqrt{1} \\ 0 & 0 & 0 & 0 \\ 0 & 0 & 0 & 0 \end{pmatrix},$$

$$\hat{A}_i^\dagger = (\hat{I}_s \otimes \hat{A}_i)^\dagger = \begin{pmatrix} 0 & 0 & 0 & 0 \\ \sqrt{1} & 0 & 0 & 0 \\ 0 & 0 & 0 & 0 \\ 0 & 0 & \sqrt{1} & 0 \end{pmatrix}, \tag{4}$$

or for matrix elements:

$$(\hat{A}_s)^{jk} = \begin{cases} \sqrt{1}, & k - j = 2 \\ 0, & k - j \neq 2 \end{cases}, \ j, k = \overline{1, 4},$$

$$(\hat{A}_s^\dagger)^{jk} = \begin{cases} \sqrt{1}, & j - k = 2 \\ 0, & j - k \neq 2 \end{cases}, \ j, k = \sqrt{1, 4},$$

$$(\hat{A}_i)^{jk} = \begin{cases} \sqrt{1}, & k - j = 1 \text{ and } k \bmod 2 = 0 \\ 0, & k - j \neq 1 \text{ or } k \bmod 2 \neq 0 \end{cases}, \ j, k = \overline{1, 4},$$

$$(\hat{A}_i^\dagger)^{jk} = \begin{cases} \sqrt{1}, & j - k = 1 \text{ and } j \bmod 2 = 0 \\ 0, & j - k \neq 1 \text{ or } j \bmod 2 \neq 0 \end{cases}, \ j, k = \overline{1, 4}.$$

2.3. Averaging over the initial vacuum state

The correlation function of the amplitudes of the signal and idle beams has the form

$$\langle E_s(\mathbf{r}_\perp) E_i(\mathbf{r}'_\perp) \rangle = N^2 \langle 00 | \hat{A}_s^{(\text{out})}(\mathbf{r}_\perp) \hat{A}_i^{(\text{out})}(\mathbf{r}'_\perp) | 00 \rangle, \tag{5}$$

where N — is a constant coefficient, and $\hat{A}_s^{(\text{out})}(\mathbf{r}_\perp) \cdot \hat{A}_i^{(\text{out})}(\mathbf{r}'_\perp)$ — the usual product of operators. The same correlation function was used in [9] to evaluate the quality of phantom images in the case of a three-photon process.

From (3) and (5) it turns out that to solve the problem you need to find only one matrix element $(j, k) = (1, 1)$:

$$\langle \hat{A}_s^{(\text{out})}(\mathbf{r}_\perp) \hat{A}_i^{(\text{out})}(\mathbf{r}'_\perp) \rangle = \left(\hat{A}_s^{(\text{out})}(\mathbf{r}_\perp) \hat{A}_i^{(\text{out})}(\mathbf{r}'_\perp) \right)^{11}$$

$$= \sum_{k=1}^{4} (A_s^{(\text{out})})^{1k} (A_i^{(\text{out})})^{k1} = \sum_{k=1}^{4} (A_s^{(\text{out})})^{1k} (A_i^{\dagger(\text{out})})^{1k}. \tag{6}$$

Let us write down a system of equations (2) for matrix elements:

$$\begin{cases} \frac{\partial A_s^{jk}}{\partial z} = \chi^{(3)} A_p(\mathbf{r}) A_q(\mathbf{r}) (A_i^\dagger)^{jk}, \\ \frac{\partial (A_i^\dagger)^{jk}}{\partial z} = -\chi^{(3)} A_p(\mathbf{r}) A_q(\mathbf{r}) A_s^{jk}, \ j, k = \overline{1, 4}. \end{cases}$$

The initial conditions are matrix elements of operators (4).

It follows from (6) that it is necessary to find solutions for the first rows of matrices, and from (4) it is clear that only two systems of differential equations need to be solved, since the systems of equations for other matrix elements have trivial solutions:

$$\begin{cases} \frac{\partial A_s^{13}}{\partial z} = \chi^{(3)} A_p(\mathbf{r}) A_q(\mathbf{r}) (A_i^\dagger)^{13}, \\ \frac{\partial (A_i^\dagger)^{13}}{\partial z} = -\chi^{(3)} A_p(\mathbf{r}) A_q(\mathbf{r}) A_s^{13}, \\ A_s^{13}|_{z=-l_z} = 1, \\ (A_i^\dagger)^{13}|_{z=l_z} = 0, \end{cases}$$

$$\begin{cases} \frac{\partial A_s^{21}}{\partial z} = \chi^{(3)} A_p(\mathbf{r}) A_q(\mathbf{r}) (A_i^\dagger)^{21}, \\ \frac{\partial (A_i^\dagger)^{21}}{\partial z} = -\chi^{(3)} A_p(\mathbf{r}) A_q(\mathbf{r}) A_s^{21}, \\ A_s^{21}|_{z=-l_z} = 0, \\ (A_i^\dagger)^{21}|_{z=l_z} = 1. \end{cases} \tag{7}$$

Then the expression (6) is converted to the form

$$\langle \hat{A}_s^{(\text{out})}(\mathbf{r}_\perp) \hat{A}_i^{(\text{out})}(\mathbf{r}'_\perp) \rangle = A_s^{13}|_{z=l_z} (A_i^\dagger)^{13}|_{z=-l_z} + A_s^{21}|_{z=l_z} (A_i^\dagger)^{21}|_{z=-l_z}. \tag{8}$$

The correlation function of the amplitudes of the signal and idle beams, which determines the phantom image, in the case of neglect of diffraction in a nonlinear medium is equal to

$$G(\mathbf{r}_\perp, \mathbf{r}'_\perp) = N^4 \left| \int h_1(\mathbf{r}'_\perp, \mathbf{r}''_\perp) h_2(\mathbf{r}_\perp, \mathbf{r}''_\perp) \right.$$

$$\left. \times \langle \hat{A}_s^{(\text{out})}(\mathbf{r}''_\perp) \hat{A}_i^{(\text{out})}(\mathbf{r}'''_\perp) \rangle \delta(\mathbf{r}''_\perp - \mathbf{r}'''_\perp) d\mathbf{r}''_\perp d\mathbf{r}'''_\perp \right|^2.$$

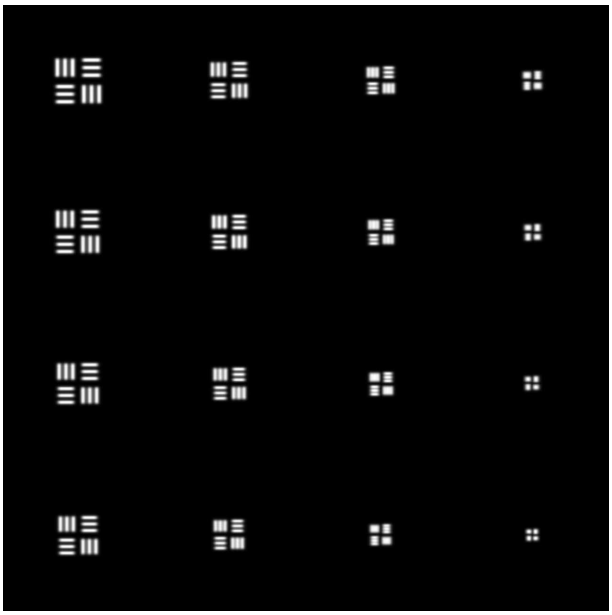

Figure 2. A phantom image of a standard test target with the following parameter values: $\sigma_y = \sigma_z = 2\,\text{mm}$, $\chi^{(3)}A_pA_q = 0.3\,\text{mm}^{-1}$, $l_x = l_y = l_z = 3\,\text{mm}$, $f = 1\,\text{m}$. The distance between the slits is from 0.02 to 0.08 mm in increments of 0.004 mm. The wavelength is $0.702\,\mu\text{m}$. The test target size is $6 \times 6\,\text{mm}$.

Channel propagators, in contrast to [9], will be written in the Kirchhoff approximation, since we assume to work with relatively large numerical apertures when the Fresnel approximation may become inadequate:

$$h_1(\mathbf{r}'_\perp, \mathbf{r}''_\perp) = \frac{k}{2\pi i} T(\mathbf{r}') \frac{\exp[ik\sqrt{\|\mathbf{r}'_\perp - \mathbf{r}''_\perp\|^2 + f^2}]}{\sqrt{\|\mathbf{r}'_\perp - \mathbf{r}''_\perp\|^2 + f^2}} \times \exp\left[-\frac{ik\|\mathbf{r}''_\perp\|^2}{2f}\right],$$

$$h_2(\mathbf{r}_\perp, \mathbf{r}''_\perp) = \frac{k}{2\pi i} \frac{\exp[ik\sqrt{\|\mathbf{r}_\perp - \mathbf{r}''_\perp\|^2 + f^2}]}{\sqrt{\|\mathbf{r}_\perp - \mathbf{r}''_\perp\|^2 + f^2}} \times \exp\left[-\frac{ik\|\mathbf{r}''_\perp\|^2}{2f}\right].$$

Here $T(\mathbf{r}')$ — the amplitude transmission function of the object, f — the focal length of the lenses L.

3. Calculation results

To analyze the phantom image, we took a standard test target as an object. It represents contrasting black and white strokes of different frequency and direction. By which squares of strokes are distinguishable in the image, the quality of the latter is determined. Unit of measurement — number of distinguishable strokes per mm. Different directions of strokes are important for assessing the possible astigmatism of the optical system under study.

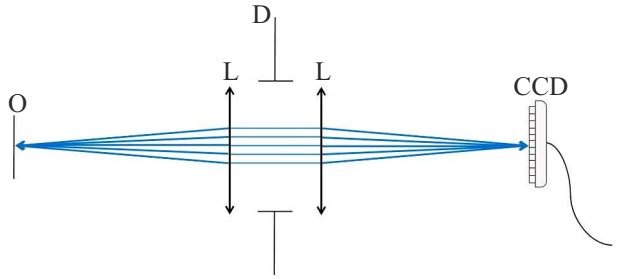

Figure 3. Equivalent linear optical system.

In our case, as follows from Fig. 2, it appears due to unequal numerical apertures in the meridional and sagittal planes, since the orientation of the pump is such that the numerical aperture in one plane is determined by the size of the nonlinear medium, and in the other by the cross-section of the pump. We did not take into account vignetting at the edges of the field. This does not matter in principle, since our goal was to test the operability of our algorithm, although it is not difficult to take into account the decrease in the numerical aperture of inclined beams.

Using this reference image, it is easy to determine the spatial resolution of the system and evaluate its quality accordingly. In our case, this is approximately $23\,\text{mm}^{-1}$ in the meridional plane and $19\,\text{mm}^{-1}$ in the sagittal plane. Since the aperture in the meridional and sagittal planes has a different shape — rectangular and Gaussian, the ratio of these numbers does not correspond to the ratio of their linear dimensions.

4. Equivalent scheme for image quality assessment

Consider the optical scheme in Fig. 3. It is an analog of the section of Fig. 1 by the sagittal plane. The situation is as if the image of an object is simply constructed by a lens system and an ordinary linear transparent medium instead of a nonlinear one on the surface of the photodetector matrix. We will take into account the limited size of the pump by introducing a diaphragm D with a Gaussian amplitude transmission profile D. Moreover, this diaphragm is stretched across the width of the transparent medium, since the cylindrical pumping completely penetrates it in the transverse direction.

Let the object be illuminated by incoherent light. It is necessary to find the response of the optical system of the form

$$G(\mathbf{r}, \mathbf{r}') \propto \left| \int h_1(\mathbf{r}'_\perp, \mathbf{r}''_\perp) h_2(\mathbf{r}_\perp, \mathbf{r}''_\perp) D(\mathbf{r}'') d\mathbf{r}''_\perp \right|^2,$$

where the propagators

$$h_1(\mathbf{r}'_\perp, \mathbf{r}'') = \frac{k}{2\pi i} T(\mathbf{r}') \frac{\exp[ik\|\mathbf{r}' - \mathbf{r}''\|]}{\|\mathbf{r}' - \mathbf{r}''\|} \exp\left[-\frac{ik\|\mathbf{r}''_\perp\|^2}{2f}\right],$$

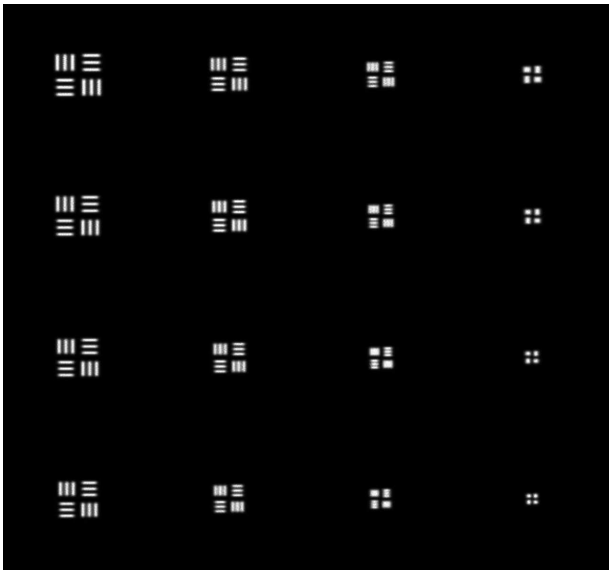

Figure 4. The test target image by an equivalent linear optical system.

$$h_2(\mathbf{r}_\perp, \mathbf{r}'') = \frac{k}{2\pi i} \frac{\exp[ik\|\mathbf{r}' - \mathbf{r}''\|]}{\|\mathbf{r}' - \mathbf{r}''\|} \exp\left[-\frac{ik\|\mathbf{r}''_\perp\|^2}{2f}\right].$$

The calculation results for an equivalent classical scheme with the same parameters are similar to the results for a four-photon system, and are shown in Fig. 4.

It can be seen that the resolution for vertical slits is less than for horizontal ones, as in the original scheme for the same reason. We also did not take into account vignetting for inclined beams.

In the equivalent scheme, the calculations are much simpler, and the result is almost the same. This is a somewhat unexpected result. It proves the equivalence of phantom nonlinear and ordinary linear optical imaging systems in terms of their quality and can be used in practical calculations.

5. Scheme with nonlinear fiber bundle

Let us consider another interesting variant of the formation of phantom images using counter four-photon mixing in a nonlinear fiber bundle (Fig. 5). In its middle, the braid is partially removed and it is irradiated by a transverse pump beam. The fibers can be, for example, made of fused quartz. Since the efficiency of the nonlinear transformation is small, almost all fibers will be equally illuminated. The spatial correlation of the signal and idle beams required for the formation of phantom images is achieved by the fact that the same number of photons will always go to both sides of the bundle due to the simultaneous birth of the signal and idle.

The right end of the harness is closely connected to the photodetector matrix, and the image of the left one with the projection lens L is formed on the object under study O, through which photons are recorded by the integrating detector BD. Thus, an algorithm for the formation of phantom images is constructively implemented, based on the spatial correlation of the transverse coordinates of the photons of the two illuminators of the object O and BD.

What are the advantages of this scheme? The quality of the images generated by it is fundamentally limited only by the pixel size, i.e. the diameter of the fiber and the corresponding size of the photodetectors in the CCD matrix. The quality of the optical system, of course, is also important, but projection systems of this class, working with a single magnification, can technically be ideal. Both ends of the light guide always provide identical illumination of both the object and the CCD photodetector matrix. There are also no diffraction distortions, because there are no fundamental limitations of the lens aperture L. All this makes the proposed scheme very attractive.

In addition, the fiber bundle can be passed into cavities that are difficult to access for direct observation, for example, the internal organs of a person. And the integrating detector can be located outside, since soft tissues are partially transparent to the red radiation of a helium-neon gas laser. The advantages of phantom images, consisting in a gentle observation mode, are fully realized at the same time.

6. Conclusion

The main result of our work is a theoretical study of the formation of phantom images in the most realistic conditions of Gaussian limited laser pumping. The results are brought to the production of computer images of objects, which can be used to assess the quality and spatial resolution, which is perhaps the main criterion for the applicability of optical systems in general. Nevertheless, it is quite obvious that the algorithm we have proposed is very complex. Therefore, for the initial evaluation analysis, we considered a simpler linear system for which, with the same initial data, we obtained

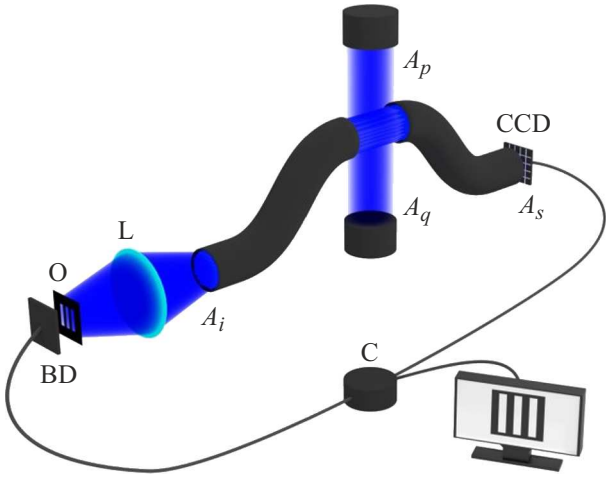

Figure 5. Scheme for the formation of phantom images using a fiber bundle.

similar computer images, thereby proving its equivalence in terms of the quality of information transmission.

Moreover, it seems to us that the use of counter four-photon mixing in the fiber-optic version has certain prospects. Here, the advantages of phantom images can be realized in full, guaranteeing both a gentle mode of observation of the objects under study and the potential possibility of penetration into cavities that are difficult to directly observe.

Acknowledgments

The authors are grateful to D.A. Balakin for his assistance in the work.

Funding

This study was supported financially by the Russian Science Foundation (project No. 21-12-00155).

Conflict of interest

The authors declare that they have no conflict of interest.

References

[1] *Kvantovoe izobrazhenie*, edited by M.I. Kolobov (original), A.S. Chirkin (translation) (Fizmatlit, M., 2009). (in Russian).
[2] M.G. Basset, F. Setzpfandt, F. Steinlechner et al. Laser & Photonics Reviews, **13**, 1900097 (2019).
[3] A.V. Belinsky. Vestnik MGU. Seriya 3. № 5, 3 (2018). (in Russian).
[4] P.-A. Moreau, P.A. Morris, E. Toninelli et al. Sci. Rep., **8**, 13183 (2018).
[5] P.-A. Moreau, P.A. Morris, E. Toninelli et al. Opt. Express., **26**, 7528 (2018).
[6] D.A. Balakin, A.V. Belinsky. Kvant. elektron., **49** (10), 967 (2019). (in Russian).
[7] D.A. Balakin, A.V. Belinsky, A.S. Chirkin. Quantum Information Processing, **18**, 80 (2019).
[8] A.V. Belinsky. Kvant. elektron., **50** (10), 951 (2020). (in Russian).
[9] D.A. Balakin, A.V. Belinsky. ZhETF, **133** (1), 26 (2021). (in Russian).
[10] A.V. Belinsky, R. Singh. ZhETF **159**, 258 (2021). (in Russian).
[11] M.P. Edgar, G.M. Gibson, M.J. Padgett. Nat. Photon., **13** (1), 13 (2019).
[12] M.F. Duarte et al. IEEE Signal Process. Mag., **25** (2), 83 (2008).
[13] Z. Zhang, X. Ma, J. Zhong. Nat. Commun., **6**, Art. no. 6225 (2015).
[14] Z. Zhang, X. Wang, G. Zheng, J. Zhong. Opt. Express, **25** (16), 19619 (2017).
[15] L. Martínez-León, P. Clemente, Y. Mori, V. Climent, J. Lancis, E. Tajahuerce. Opt. Express, **25** (5), 4975 (2017).
[16] B. Lochocki et al. Optica, **3** (10), 1056 (2016).
[17] R. Dutta et al. Biomed. Opt. Express, **10** (8), 4159 (2019).
[18] N. Radwell, K.J. Mitchell, G.M. Gibson, M.P. Edgar, R. Bowman, M.J. Padgett. Optica, **1** (5), 285 (2014).
[19] P. Clemente, V. Durán, E. Tajahuerce, P. Andrés, V. Climent, J. Lancis. Opt. Lett., **38** (14), 2524 (2013).
[20] P. Clemente, V. Durán, E. Tajahuerce, J. Lancis. Phys. Rev. A, **86** (4), Art. no. 041803 (2012).
[21] D.B. Phillips et al. Sci. Adv., **3** (4), e1601782 (2017).
[22] Z. Wei, J. Zhang, Z. Xu, Y. Liu, Y. Huang, X. Fan. IEEE Photon. J., **11** (1), 7800116 (2019).
[23] Y. Wang, F. Wang, R. Liu, P. Zhang, H. Gao, F. Li. Opt. Express, **27** (5), 5973 (2019).
[24] F. Magalhães, F.M. Araújo, M. Correia, M. Abolbashari, F. Farahi. Opt. Eng., **51** (7), 071406 (2012).
[25] K. Shibuya et al. Opt. Express, **25** (18), 21947 (2017).
[26] B. Sun et al. Science, **340** (6134), 844 (2013).
[27] Z. Zhang, S. Liu, J. Peng, M. Yao, G. Zheng, J. Zhong. Optica, **5** (3), 315 (2018).
[28] C. Zhang et al. Opt. Express, **27** (9), 13469 (2019).
[29] Z. Zhang, S. Jiao, M. Yao, X. Li, J. Zhong. Opt. Express, **26** (11), 14578 (2018).
[30] H. Wu, B. Han, Z. Wang, G. Genty, G. Feng, H. Liang. Opt. Express, **28** (7), 9957 (2020).
[31] A.V. Belinskii, D.N. Klyshko. JETP, **78**, 259 (1994).
[32] S.A. Magnitskiy, D.P. Agapov, A.S. Chirkin. Opt. Lett., **47**, 754 (2022).
[33] S.A. Magnitskiy, D.P. Agapov, I.A. Belovolov et. al. Moscow Univ. Phys. Bulletin, **76**, 424 (2021).
[34] S.A. Magnitskiy, D.P. Agapov, A.S. Chirkin. Opt. Lett., **45**, 3641 (2020).
[35] D.P. Agapov, S.A. Magnitskiy, A.S. Chirkin. Web Conf., **220**, 03002 (2019). DOI: 10.1051/epjconf/201922003002
[36] A.S. Chirkin, P.P. Gostev, D.P. Agapov, S.A. Magnitskiy. Laser Phys. Lett., **15**, 115404 (2018).
[37] A.S. Chirkin, E.V. Makeev. J. Opt. B, **5**, S500 (2005).
[38] A.V. Belinsky. ZhPS, **50** 469 (1989).(in Russian).
[39] A.S. Davydov. *Kvantovaya mekhanika* (Fizmatgiz, M., 1963). (in Russian)